Scientific Research Publishing

Open Journal of Physical Chemistry, 2021, 11, 144-156
https://www.scirp.org/journal/ojpc
ISSN Online: 2162-1977
ISSN Print: 2162-1969

Visible Light Hydrogen Evolution over α-MoO_3 and α-MoO_3/ZnO Hetero-Junction

Kahina Bounache[1], Amel Boudjemaa[1,2], Souhila Boumaza[1], Meriem Haddad[1], Warda Tallas[1], Akila Belhadi[1*], Mohamed Trari[3]

[1]Laboratory of Chemistry of Natural gas, Faculty of Chemistry, University of Science and Technology Houari Boumediene, Algiers, Algeria
[2]Centre de Recherche Scientifique et Technique en Analyses Physico-Chimique, Tipaza, Algeria
[3]Laboratory of Storage and Valorization of Renewable Energies, Faculty of Chemistry, University of Science and Technology Houari Boumediene, Algiers, Algeria
Email: *sarakila@yahoo.fr

How to cite this paper: Bounache, K., Boudjemaa, A., Boumaza, S., Haddad, M., Tallas, W., Belhadi, A. and Trari, M. (2021) Visible Light Hydrogen Evolution over α-MoO_3 and α-MoO_3/ZnO Hetero-Junction. *Open Journal of Physical Chemistry*, **11**, 144-156.
https://doi.org/10.4236/ojpc.2021.113008

Received: June 5, 2021
Accepted: July 31, 2021
Published: August 3, 2021

Abstract

MoO_3 and 5% MoO_3/ZnO were prepared by impregnation method using $(NH_4)_6Mo_7O_{24}$, $4H_2O$ as precursor and ZnO as support. The prepared samples were characterized by X-ray diffraction (XRD), scanning electronic microscopy (SEM), infra red (FTIR) and UV-Vis diffuse reflectance (DRS) spectroscopies and photo-electrochemistry. The XRD pattern showed that the MoO_3 powder treated at 700˚C is a single-phase crystallizing in an orthorhombic structure with a direct optical transition (2.70 eV). The hetero-junction 5% MoO_3/ZnO was photo-electrochemically characterized to assess its feasibility for H_2 production under visible light. The capacitance potential (C^{-2} $f(E)$) characteristic of MoO_3 plotted in Na_2SO_4, (0.1 M) electrolyte indicates n-type conduction with a flat band potential of −0.54 V_{SCE}. The photocatalytic activity was performed for the photoreduction of water to hydrogen under visible light illumination. The best performance occurs at pH ~ 7 with an evolved volume of 5.9 mL.

Keywords

MoO_3/ZnO, Hetero-Junction, Photocatalysis, Hydrogen, Visible Light

1. Introduction

Nowadays, the energy supply is becoming a major problem facing our civilization and increasing demand, leading to the exhaustion of natural resources (coal, oil, gas, etc.). For this, it is important to find friendly alternatives process for the future years. So, clean strategies are highly motivated and renewable energies

have many advantages due to their availability, cleanness and power [1]. The development of an efficient and low-cost energy carrier has recently alerted scientists to the promising approach of directly converting renewable energy into hydrogen [2] [3] [4]. This approach focuses on the H_2 production from solar energy using photo-electrochemical oxides. In this perspective, hydrogen is a promising energetic vector due to its being used as a clean status, like fuel cells, in both the transport and industrial sectors. However, it differs from other primary energetic sources in that it must be manufactured just before utilization due to the difficult storage or liquefaction. Therefore, both scientific and technological advances are being made, as it has become essential to control the technologies producing renewable and sustainable energy. Hydrogen can be produced by various methods such as water electrolysis [5] [6] [7] [8] [9], coal gasification and methane reforming (steam reforming, oxidation and dry reforming) [10] [11].

MoO_3 is an important photocatalyst that has received considerable attention as an advanced material owing to its attractive physical and chemical properties including its stability at multiple oxidation states, mechanical hardness, thermal stability, superconductivity, and great performance in many catalytic reactions [12]. Recently, numerous inspired schemes and pathways have been developed for the synthesis of nanomaterials for their potential applications in diverse technological fields [13]. Among the important transition-metal oxides such as molybdenum (Mo) based oxides are attractive due to their unique structural and optical properties [14]. Although molybdenum has oxidation states ranging from +2 to +6, oxides exist mainly in two forms namely (IV) and (VI) [15]. The existence of metal-like electronic conductivity of molybdenum(IV) oxide makes them promising in energy-related applications [16]. MoO_3 is a wide bandgap semiconductor with *n*-type behavior attributed to oxygen deficiency. Their electrochromic, thermochromic, and photochromic properties, have been investigated as smart materials for catalysis [17], sensors and lubricants. MoO_3 is also used as display devices, sensors, smart windows, lubricants, battery electrodes [17] [18] [19]. MoO_3 exhibits three crystallographic forms, orthorhombic (α-MoO_3), monoclinic (β-MoO_3), and hexagonal (θ-MoO_3) [20]. The meta-stable β and θ forms are more studied than the thermodynamically stable α-MoO_3 [21] [22]. The monoclinic variety is transformed to orthorhombic MoO_3 at 400˚C. Crystalline o-MoO_3 has a layered structure of distorted MoO_6 polyhedral sharing edges and corners and one oxygen in each polyhedron is unshared M = O. It is literally known that the phase purity of MoO_3 relied on the adopted synthetic procedure and experimental conditions. Considerable progress has been accomplished recently for the size and phase-controlled synthesis of MoO_3 with optimized catalytic properties [23] [24]. There are many routes based on different starting compounds: polymerization and polycondensation of metal alkoxides, ion-exchange methods and oxidizing reaction of metallic W or Mo with a solution of H_2O [25] [26].

ZnO is *n-type* semiconductor with a direct wide bandgap energy of ~3.3 eV and large exciton binding energy (60 meV) at room temperature [27]. Its good optical and electrical properties coupled with a low cost, non-toxicity and abundance in nature make it attractive in photo-electrochemical conversion. Its other favorable properties include electrochemical stability and thermal stability as well as good stability in hydrogen plasma [28]. So, the control of size and shape of ZnO nano/micro-structures is becoming an interesting field due to their inherent size and shape-dependent applications [29] [30]. Its unique properties and low production cost make it attractive in chemicals, semiconductors, electronics, and health care industries.

The improvement of ZnO conductivity is commonly done through doping by hetero-valent atoms or oxygen deficiency. Such operations depend on the type of dopant or surrounding atmosphere, to increase the density of free charge carriers [31] [32] [33].

The aim of the present work is focused on the preparation of α-MoO_3 and the hetero-junction α-5%MoO_3/ZnO by impregnation method. The photocatalysts properties were assessed through the hydrogen formation upon visible light. The materials were characterized by XRD, FT-IR, DRS, SEM analysis, and the photo-electrochemistry.

2. Experimental Part

2.1. Materials Preparation

The support ZnO was prepared by nitrate route at pH ~ 10 using $Zn(NO_3)_2$, $6H_2O$ as precursor material. The solution was slowly evaporated and the obtained solid is heated, at 500˚C (6 h) with a flow rate of 5˚C/min. The supported material 5 wt% MoO_3/ZnO was synthesized by wet impregnation using $(NH_4)_6Mo_7O_{24}$, $4H_2O$ on ZnO support. The suspension was agitated for 1 h, evaporated on a sand bath and dried at 100˚C overnight. Finally, all the samples were calcined at 700˚C for 6 h.

2.2. Characterization Technique

The solides MoO_3 and 5% MoO_3/ZnO were identified by X ray diffraction (XRD) using INEL XRG 3000 diffractometer with CuKα anticathode (λ = 0.15405 nm). Scanning electronic microscopy (SEM) study was carried out with Philips XL30-FEG equipment. The FTIR spectra were recorded with a FTIR Alpha Bruckers spectrometer. UV-Vis diffuse reflectance spectra (DRS) were measured in the range of 200 - 900 nm using a Specord 200 Plus spectrophotomoter with an integrating sphere accessory. The reflectance (R) was converted to absorbance by Kubelka-Munk function:

$$F(R) = (1-R)^2 / 2R \quad (1)$$

The photo-electrochemical study was performed in standard cell with three electrodes; Pt auxiliary electrode, a saturated calomel electrode (SCE) and the working electrode. The studies were inverstigated in neutral electrolyte recorded

PGZ301 potentiostat (Radiometer analytical) using Na_2SO_4 (0.1 M). The capacitance-potential (C^{-2} *f*(*E*)) characterization carried out at a frequency of 10 kHz.

2.3. Photocatalytic Application

The photocatalytic activity of different samples was assessed by the reduction of water to hydrogen under three tungsten lamps (3 × 200 W). The reaction war realized in a Pyrex double walled reactor equipped with a cooling system; the temperature was regulated at 50˚C ± 1˚C. Typically, 100 mg photocatalysis were suspended in 200 mL of Na_2SO_4 aqueous solution (0.1 M). The suspension was bulbbed with nitrogen for 30 min. The hydrogen was quantified volumetrically by water displacement caused by the pressure developed inside the reactor. The gas (H_2) generated was identified by gas chromatography (Agilent Technologies 7890A, GC system) analysis with the retention time of 1.592 mn.

3. Results and Discussion

3.1. Characterization

Figure 1 displays the XRD results for the samples calcined at 700˚C. All characteristic peaks located at 24.1˚, 26.5˚, 28.16˚, 34.2˚, 39.4˚, 49.8˚ and 59.5˚ indicate that α-MoO_3 crystallizes in the orthorhombic system (JCPDS Card N˚ 47-1320) with no impurity. The 2θ peak at 12.8˚ indicates the presence of the orthorhombic phase instead of the monoclinic structure [34].

Figure 1 shows the formation of the zincite phase in agreement with the JCPDS Card N˚ 36-1451. For the system 5 wt% MoO_3/ZnO, the presence of the mixed phases confirms the formation of the hetero-junction. The mean particle sizes (*D*) are evaluated using the broadening of intense XRD peaks (β):

$$D = 0.9\lambda\left\{\beta\cos\theta\right\}^{-1} \tag{2}$$

D is found to be 84 nm. The lattice parameters *a* and *c* was calculated using Equation (2):

$$d_{hkl}^2 = 4/3\left(\left(h^2 + hk + k^2\right)/a^2\right)l^2/c^2 \tag{3}$$

where d_{hkl} is the inter planar spacing obtained from Bragg's law, and *h, k and l* the Miller indices. The lattice parameters are accurately evaluated by the least square method: *a* = 3.89 and *c* =7.09 Å, which are slightly higher than those for bulk ZnO (*a* = 3.16 Å and *c* = 5.1 Å), may be due to the effects of compressive grains.

The surface morphology of the synthesized samples was observed by the SEM analysis. MoO_3 has a fairly homogeneous structure and a stick-like appearance (Figure 2(a)). ZnO has a homogeneous structure and a spherical appearance (Figure 2(b)). The SEM image shows that the system 5 wt% MoO_3/ZnO has a homogeneous nature with spherical form and regular sizes (Figure 2(c)). It has been observed the grain size of the ZnO changes with doping of Mo.

The FT-IR spectra of MoO_3 and Mo-doped ZnO are regrouped in Figure 3.

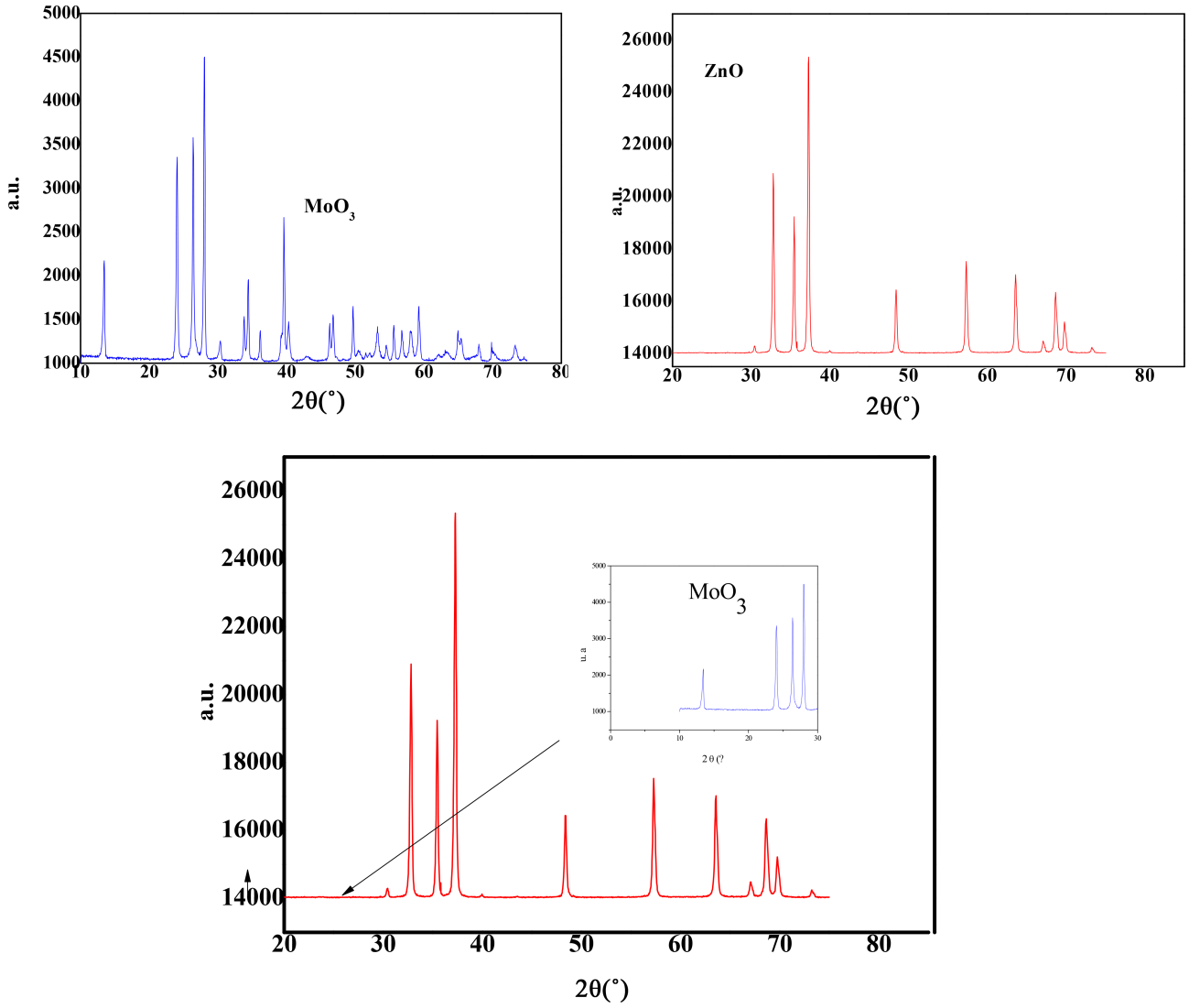

Figure 1. XRD patterns of MoO_3, ZnO and 5% MoO_3/ZnO.

The peak at 1600 cm^{-1} is assigned to the bending vibration of adsorbed water on the material surface while the peak around 420 cm^{-1} is attributed to the stretching vibration of Zn-O bonds. The presence of MoO_3 depicted evidenced by peaks at 980, 819 and 453 cm^{-1}. The first peak characteristic of the terminal M = O stretching vibration with an indicator of the layered orthorhombic MoO_3 phase. The peak at 819 cm^{-1} is assigned to the stretching mode of oxygen in Mo-O-Mo bonds, while the broad band at 453 cm^{-1} to the bending vibration of oxygen atom are linked to three metal atoms. Two peaks at 1544 cm^{-1} and 1442 cm^{-1} could be ascribed to the formation of Mo-O-Zn bond. The presence of additional absorption bands in the region (404 - 1110 cm^{-1}) compared to ZnO nanoparticles indicates the presence of Mo-oxides. The M-O frequencies observed for metal oxides are in agreement with the literature [35] [36].

The optical band gap (E_g) is estimated by assuming a transition between the valence and the conduction bands using the relation:

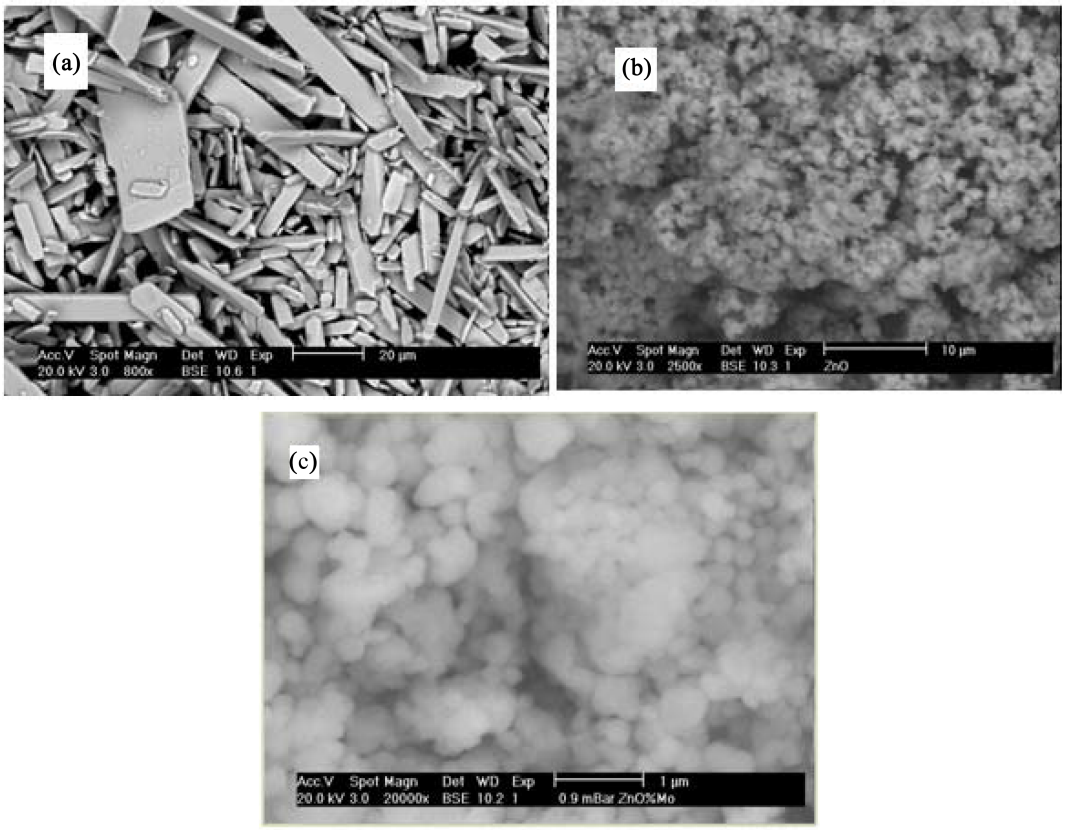

Figure 2. SEM images of (a) MoO_3, (b) ZnO and (c) of 5% MoO_3/ZnO.

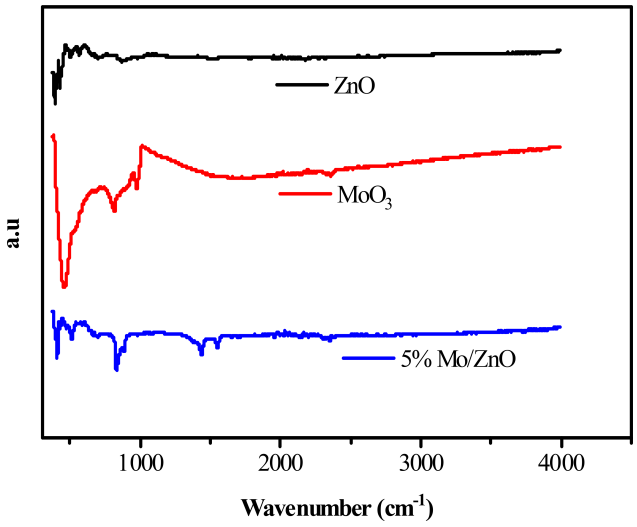

Figure 3. FTIR spectra of MoO_3 and 5% MoO_3/ZnO prepared at 700˚C.

$$(\alpha h\nu)^n = B \times (h\nu - E_g) \tag{4}$$

where $h\nu$ is the energy of the incident photon and B is an energy-independent constant. For allowed direct transitions the coefficient n is equal to 2 and for indirect allowed transitions $n = 1/2$. So, the gap E_g of MoO_3 is found to be 2.70 eV (**Figure 4**) from the plot of $(\alpha h\nu)^{1/2}$ versus $h\nu$ and by extrapolating the li-

near portion of the absorption edge to $(\alpha h\nu)^{1/2} = 0$ [37]. This value is in agreement with the yellow color of the material. ZnO exhibits an indirect transition with a band gap of 3.10 eV (**Figure 4**).

The photo-electrochemical (PEC) characterization was performed in the dark and under irradiation at a scan rate of 10 mV s^{-1} in the region [−1, 1 V]. The study was conducted in the same conditions of the photo-catalytic tests (see below). A good electrochemical stability of the material is observed with a dark current (J_d) less than 2 mA/cm^2. The increase of the photo-current (J_{ph}) along the anodic polarization is characteristic of *n*-type conductivity where the electrons are the majority charges carriers (**Figure 5**). The potential of H_2O/H_2 couple is −0.48 and −0.49 V respectively onto MnO_3 and ZnO. The value is obtained by extrapolating the tangent line over the slope and prolonging it to zero current in the current-potential curve.

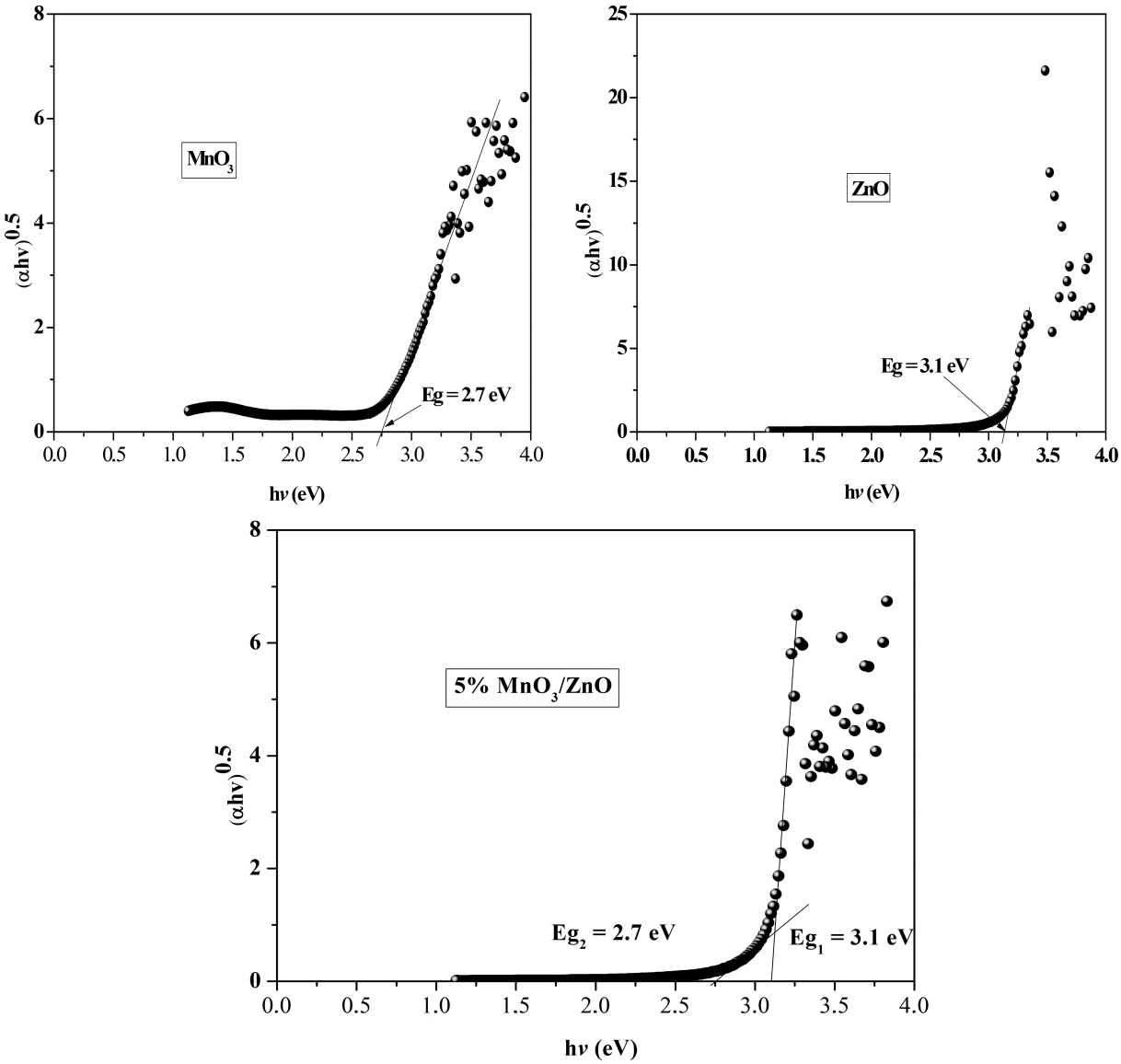

Figure 4. Indirect band gap transition of MnO_3, ZnO and 5% MnO_3/ZnO.

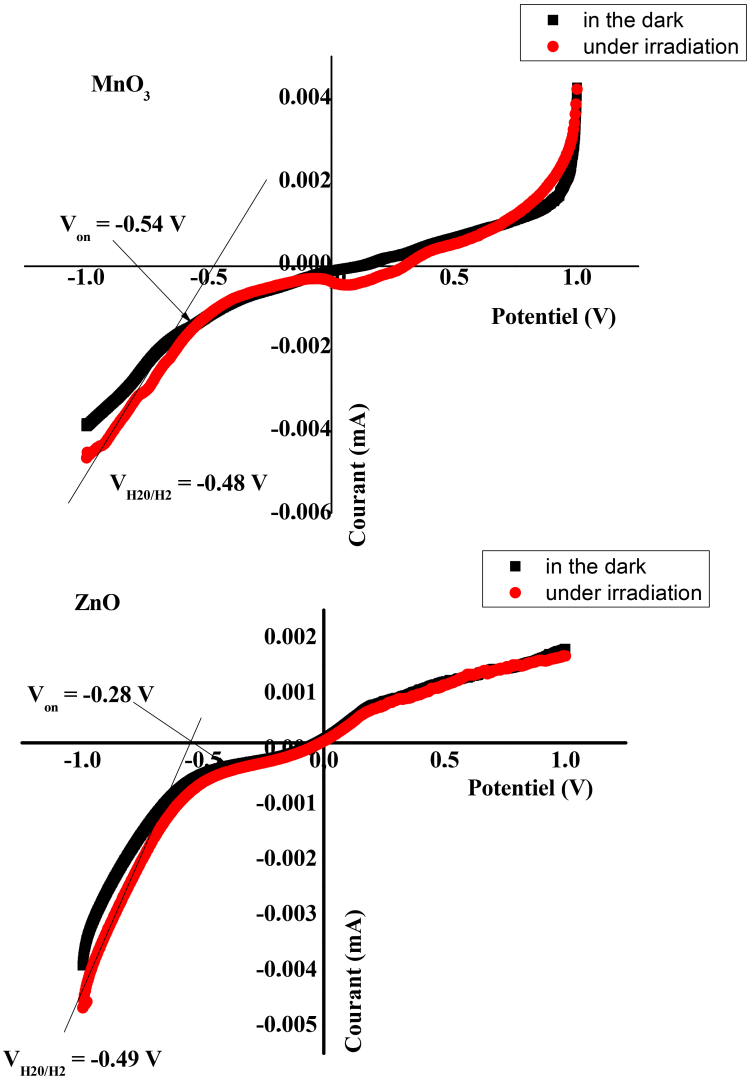

Figure 5. Current-potential characteristics of MoO_3 and ZnO photocatalyst in Na_2SO_4 solution.

The (C^{-2} *f*(*E*)) plot of the semi-conductor/electrolyte junction is regrouped in Figure 6. The potential V_{fb} is obtained according to the following equation:

$$\frac{1}{C^2} = \frac{2}{\varepsilon\varepsilon_o e N_D}\left(V - V_{fb} - \frac{kT}{e}\right) \tag{5}$$

where e is electron charge (1.6×10^{-19} C), ε the dielectric constant, and N_D the electrons density.

The positive slopes indicating *n* type [38] behavior where the majority charges carriers are electrons. The potential E_{fb} of MnO_3 and ZnO is 0.61 and −0.61 V, respectively, these values are derived from the potential intercept of potential axis ($C^{-2} = 0$).

3.2. Photocatalytic Hydrogen Generation

The synthesized photocatalysts are successfully applied for H_2 production under

visible light irradiation in neutral solution (0.1 M Na_2SO_4) using $S_2O_3^{2-}$ as hole scavenger (10^{-3} M) under magnetic stirring (200 rpm). It is shown that the H_2 production over MoO_3 and 5 wt% MoO_3/ZnO as a function of the catalyst mass in the range (50 - 300 mg) indicated that a maximum is reached with a catalyst mass of 200 mg. The H_2 amount is 5.9 mL for MoO_3 and 2.4 mL for 5 wt% MoO_3/ZnO (Figure 7). The low value of H_2 produced over the heterosystem indicated the absence of synergetic effect between MoO_3 and ZnO. The enhanced photoactivity of MoO_3 under visible illumination can be attributed to the defect states introduced within the gap region during the mechanical treatment on the catalyst surface. However, the problem is that such defect sates can also work as carriers traps, thereby yielding a decrease of the quantum yields

Figure 8 regrouped the results of the hydrogen generation of versus pH with the catalyst mass of 200 mg for three different pHs (~ 7, 10 and 12) in presence of $S_2O_3^{2}$ as hole scavenger. So, H_2 evolution decreases with raising pH and the

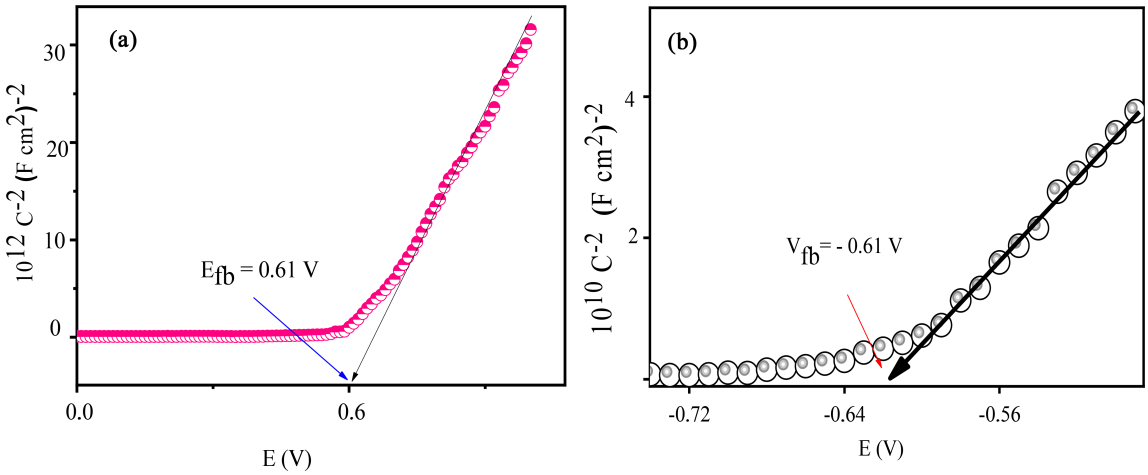

Figure 6. The capacitance-potential $C^{-2}f(E)$ plot of MoO_3 (a) and ZnO (b) calcined at 700˚C in neutral solution (Na_2SO_4, 0.1 M).

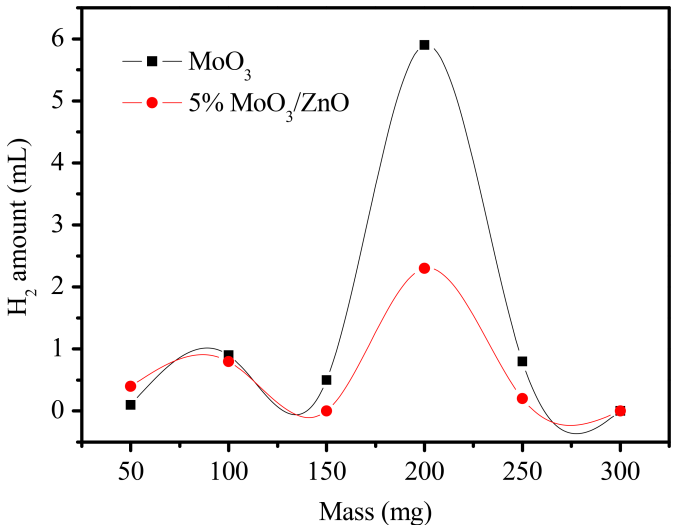

Figure 7. H_2-Evolution on MoO_3 and 5% MoO_3/ZnO as a function of the catalyst mass.

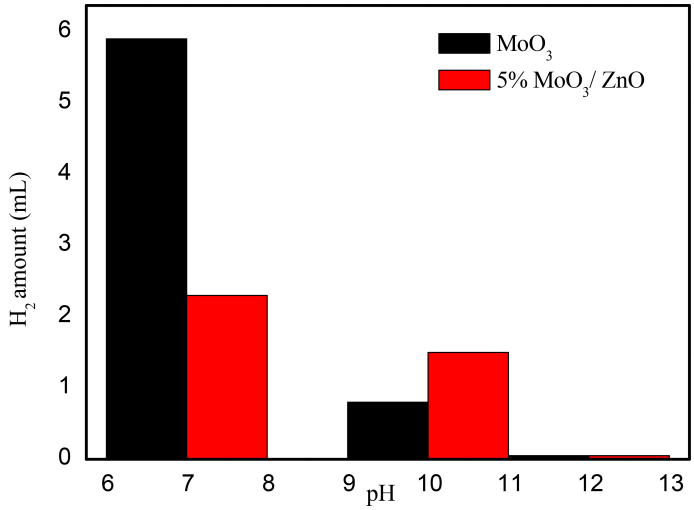

Figure 8. H_2-Evolution on MoO_3 and 5% MoO_3.

best photoactivity is obtained on MoO_3 at pH ~ 7 while on the hetero-junction 5 wt% MoO_3/ZnO only 1.4 mL is obtained at pH 10. The photocatalytic performance of MoO_3 is close to the work on delafossite reported by Bellal *et al.* [39].

4. Conclusion

The photocatalytic hydrogen generation was evaluated using the synthesized α-MoO_3, ZnO and their hetero-junction. The prepared materials were characterized by XRD, FT-IR, UV-Vis DRS, SEM and photo-electrochemical analysis. The operating conditions were optimized to improve the hydrogen generation under visible light, and the best photo-activity was observed with a catalyst mass of 200 mg in Na_2SO_4 solution. It was found that α-MoO_3 has the potential to produce hydrogen compared to the heterojunction due to both the light absorption in the visible region and the absence of synergy.

Acknowledgements

The authors thank Dr. A. Djadoun and Dr. R. Brahimi for their technical assistance. The financial support of this work is provided by the Faculty of Chemistry.

Conflicts of Interest

The authors declare no conflicts of interest regarding the publication of this paper.

References

[1] Aouali, F.Z., Becherif, M., Ramadan, H.S., Emziane, M., Khellaf, A. and Mohammedi, K. (2017) Analytical Modelling and Experimental Validation of Proton Exchange Membrane Electrolyser for Hydrogen Production. *International Journal of Hydrogen Energy*, **42**, 1366-1374. https://doi.org/10.1016/j.ijhydene.2016.03.101

[2] Grätzel, M. (2001) Photoelectrochemical Cells. *Nature*, **414**, 338-344. https://doi.org/10.1038/35104607

[3] Walter, M.G., Warren, E.L., McKone, J.R., Boettcher, S.W., Mi, Q.X., Santori, E.A. and Lewis, N.S. (2010) Solar Water Splitting cells. *ACS Publications*, **110**, 6446-6473. https://doi.org/10.1021/cr1002326

[4] Tachibana, Y., Vayssieres, L. and Durrant, J.R. (2012) Artificial photosynthesis for solar water-splitting. *Nature Photonics*, **6**, 511-518. https://doi.org/10.1038/nphoton.2012.175

[5] Belhadi, A., Nadjem, I., Zaidat, S., Boudjemaa, A. and Trari, M. (2015) Hydrogen Evolution under Visible Light over the Heterojunction p-CuO/n-ZnO Prepared by Impregnation Method. *International Journal of Energy Research*, **39**, 1909-1916. https://doi.org/10.1002/er.3386

[6] Han, Z., Qiu, F., Eisenberg, R., Holland, P.L. and Krauss, T.D. (2012) Robust Photogeneration of H_2 in Water Using Semi-Conductor Nanocrystals and a Nickel Catalyst. *Science*, **80**, 1321-1324. https://doi.org/10.1126/science.1227775

[7] Tebibel, H., Khellaf, A., Menia, S. and Nouicer, I. (2017) Design, Modelling and Optimal Power and Hydrogen Management Strategy of an off Grid PV System for Hydrogen Production Using Methanol Electrolysis. *International Journal of Hydrogen Energy*, **42**, 14950-14967. https://doi.org/10.1016/j.ijhydene.2017.05.010

[8] Boumaza, S., Belhadi, A., Doulache, M. and Trari, M. (2012) Photocatalytic Hydrogen Production over NiO Modified Silica under Visible Light Irradiation. *International Journal of Hydrogen Energy*, **37**, 4908-4914. https://doi.org/10.1016/j.ijhydene.2011.12.116

[9] Menia, S., Tebibel, H., Lssouane, F., Khellaf, A. and Nouicer, I. (2017) Hydrogen Production by Methanol Aqueous Electrolysis Using Photovoltaic Energy, Algerian Potential. *International Journal of Hydrogen Energy*, **42**, 8661-8669. https://doi.org/10.1016/j.ijhydene.2016.11.178

[10] Belhadi, A., Boumaza, S., Djadoun, A., Trari, M. and Cherifi, O. (2016) Methane Steam Reforming on Supported Nickel, Effect of Nickel Content for Product Hydrogen. *Open Journal of Physical Chemistry*, **6**, 34-41. https://doi.org/10.4236/ojpc.2016.62003

[11] Touahra, F., Sehailia, M., Halliche, D., Bachari, K., Saadi, A. and Cherifi, O. (2016) (MnO/Mn_3O_4)-NiAl Nanoparticles as Smart Carbon Resistant Catalysts for the Production of Syngas by Means of CO_2 Reforming of Methane, Advocating the Role of Concurrent Carbothermic Redox Looping in the Elimination of Coke. *International Journal of Hydrogen Energy*, **41**, 21140-21156. https://doi.org/10.1016/j.ijhydene.2016.08.194

[12] Enneti, R.K. and Wolfe, T.A. (2012) Agglomeration during Reduction of MoO_3. *International Journal of Refractory Metals and Hard Materials*, **31**, 47-50. https://doi.org/10.1016/j.ijrmhm.2011.09.004

[13] Patzke, G.R., Krumeich, F. and Nesper, R. (2002) Oxidic Nanotubes and Nanorods—Anisotropic Modules for a Future Nanotechnology. *Angewandte Chemie International Edition*, **41**, 2446-2461. https://doi.org/10.1002/1521-3773(20020715)41:14<2446::AID-ANIE2446>3.0.CO;2-K

[14] Hamelmann, F., Gesheva, K., Ivanova, T., Szekeres, A., Abroshev, M. and Heinzmann, U. (2005) Optical and Electrochromic Characterization of Multilayered Mixed Metal Oxide Thin Films. *The Journal of Optoelectronics and Advanced Materials*, **7**, 393-399.

[15] Rabalais, J.W., Colton, R.J. and Guzman, A.M. (1974) Trapped Electrons in Substoichiometric MoO_3 Observed by X-Ray Electron Spectroscopy. Chemical Physics

Letters, **29**, 131-133. https://doi.org/10.1016/0009-2614(74)80149-1

[16] Ellefson, C.A., Marin-Flores, O., Ha, S. and Norton, M.G. (2012) Synthesis and Applications of Molybdenum (IV) Oxide. *Journal of Materials Science*, **47**, 2057-2071. https://doi.org/10.1007/s10853-011-5918-5

[17] Debecker, D.P., Stoyanova, M., Rodemerck, U. and Gaigneaux, E.M. (2010) Facile Preparation of MoO_3/SiO_2-Al_2O_3 Olefin Metathesis Catalysts by Thermal Spreading, *Studies in Surface Science and Catalysis*, **175**, 581-585. https://doi.org/10.1016/S0167-2991(10)75113-2

[18] Youn-Su, K., Hyo-Jin, A., Hee-Sang, S., Hoon, N.S., Tae-Yeon, S. and Bae, K.W. (2007) Pt-Embedded MoO_3 Electrodes For Rechargeable Lithium Batteries. *Electrochemical and Solid-State Letters*, **10**, 180-183. https://doi.org/10.1149/1.2739212

[19] Ghorai, T.K., Dhak, D., Biswas, S.K., Dalai, S. and Pramanik, P. (2007) Photocatalytic Oxidation of Organic Dyes by Nano-Sized Metal Molybdate Incorporated Titanium Dioxide ($M_xMo_xTi_{1-X}O_6$) (M = Ni, Cu, Zn) Photocatalysts. *Journal of Molecular Catalysis A*, *Chemical*, **273**, 224-229. https://doi.org/10.1016/j.molcata.2007.03.075

[20] Lou, X.W. and Zeng, H.C. (2002) Hydrothermal Synthesis of α-MoO_3 Nanorods via Acidification of Ammonium Heptamolybdate Tetrahydrate. *Chemistry of Materials*, **14**, 4781-4789. https://doi.org/10.1021/cm0206237

[21] Song, J., Ni, X., Zhang, D. and Zheng, H. (2006) Fabrication and Photoluminescence Properties of Hexagonal MoO_3 Rods. *Solid State Sciences*, **8**, 1164-1167. https://doi.org/10.1016/j.solidstatesciences.2006.05.002

[22] Mahajan, S.S., Mujawar, S.H., Shinde, P.S., Inamdar, A.I. and Patil, P.S. (2008) Concentration Dependent Structural, Optical and Electrochromic Properties of MoO_3 Thin Films. *International Journal of Electrochemical Science*, **3**, 953-960.

[23] Chithambararaj, A. and Chandra, B.A. (2011) Hydrothermal Synthesis of Hexagonal and Orthorhombic MoO_3 Nanoparticles. *Journal of Alloys and Compounds*, **509**, 8105-8110. https://doi.org/10.1016/j.jallcom.2011.05.067

[24] Chithambararaj, A. and Chandra, B.A. (2011) Investigation on Structural, Thermal, Optical and Sensing Properties of Meta-Stable Hexagonal MoO_3 Nanocrystals of One Dimensional Structure. *Beilstein Journal of Nanotechnology*, **2**, 585-592. https://doi.org/10.3762/bjnano.2.62

[25] Agrawal, A., Cronin, J.P. and Zhang, R. (1993) Review of Solid State Electrochromic Coatings Produced Using Sol-Gel Techniques. *Solar Energy Materials & Solar Cells*, **31**, 9-21. https://doi.org/10.1016/0927-0248(93)90003-L

[26] Zhang, Y., Kuai, S., Wang, Z. and Hu, X. (2000) Preparation and Electrochromic Properties of Li-Doped MoO_3 Films Fabricated by the Peroxo Sol-Gel Process. *Applied Surface Science*, **165**, 56-59. https://doi.org/10.1016/S0169-4332(00)00369-X

[27] Shinde, S.S., Shinde, P.S., Oh, Y.W., Haranath, D., Bhosale, C.H. and Rajpure, K.Y. (2012) Structural, Optoelectronic, Luminescence and Thermal Properties of Ga-Doped Zinc Oxide Thin Films. *Applied Surface Science*, **258**, 9969-9976. https://doi.org/10.1016/j.apsusc.2012.06.058

[28] Muiva, C.M., Sathiaraj, T.S. and Maabong, K. (2011) Effect of Doping Concentration on the Properties of Aluminium Doped Zinc Oxide Thin Films Prepared by Spray Pyrolysis for Transparent Electrode Applications. *Ceramics International*, **37**, 555-560. https://doi.org/10.1016/j.ceramint.2010.09.042

[29] Hossain, M.F., Zhang, Z.H. and Takahashi, T. (2010) Novel Micro-Ring Structured ZnO Photoelectrode for Dye-Sensitized Solar Cell. *Nano-Micro Letters*, **2**, 53-55.

https://doi.org/10.1007/BF03353618

[30] Piccinno, F., Gottschalk, F., Seeger, S. and Nowack, B. (2012) Industrial Production Quantities and Uses of Ten Engineered Nanomaterials in Europe and the World. *Journal of Nanoparticle Research*, **14**, 1109-1120. https://doi.org/10.1007/s11051-012-1109-9

[31] Wu, M., Yu, S., Chen, G., He, L., Yang, L. and Zhang, W. (2015) Structural, Optical, and Electrical Properties of Mo-Doped ZnO Thin Films Prepared by Magnetron Sputtering. *Applied Surface Science*, **324**, 791-796. https://doi.org/10.1016/j.apsusc.2014.11.039

[32] Chen, S., Warwick, M.E.A. and Binions, R. (2015) Effects of Film Thickness and Thermal Treatment on the Structural and Opto-Electronic Properties of Ga-Doped ZnO Films Deposited by Sol-Gel Method. *Solar Energy Materials and Solar Cells*, **137**, 202-209. https://doi.org/10.1016/j.solmat.2015.02.016

[33] Karamat, S., Rawat, R.S., Lee, P., Tan, T.L. and Ramanujan, R.V. (2014) Structural, Elemental, Optical and Magnetic Study of Fe Doped ZnO and Impurity Phase Formation. *Progress in Natural Science*, *Materials International*, **24**, 142-149. https://doi.org/10.1016/j.pnsc.2014.03.009

[34] Mizushima, T., Fukushima, K., Ohkita, H. and Kakuta, N. (2007) Synthesis of β-MoO_3 through Evaporation of HNO_3-Added Molybdic Acid Solution and Its Catalytic Performance in Partial Oxidation of Methanol. *Applied Catalysis A*: *General*, **326**, 106-112. https://doi.org/10.1016/j.apcata.2007.04.006

[35] Venkatachalam, N., Palanichany, M., Banumathi, A. and Murugesan, V. (2007) Enhanced Photocatalytic Degradation of 4-Chlorophrnol by Zr^{4+} Doped Nano TiO_2. *Journal of Molecular Catalysis A*: *Chemical*, **266**, 158-165. https://doi.org/10.1016/j.molcata.2006.10.051

[36] Song, J., Ni, X., Gao, L. and Zheng, H. (2007) Synthesis of Metastable h-MoO_3 by Simple Chemical Precipitation. *Materials Chemistry and Physics*, **102**, 245-248. https://doi.org/10.1016/j.matchemphys.2006.12.011

[37] He, T. and Yao, J. (2003) Photochromism of Molybdenum Oxide. *Journal of Photochemistry and Photobiology C*: *Photochemistry Reviews*, **4**, 125-143. https://doi.org/10.1016/S1389-5567(03)00025-X

[38] Dipanjan, M., Karmakar, K. and Mandal, K. (2019) N-N Type Core-Shell Heterojunction Engineering with MoO_3 over ZnO Nanorod Cores for Enhanced Solar Energy Harvesting Application in a Photoelectrochemical Cell. *Journal of Alloys and Compounds,* **791**, 739-746. https://doi.org/10.1016/j.jallcom.2019.03.292

[39] Bellal, B., Saadi, S., Koriche, N., Bouguelia, A. and Trari, M. (2009) Physical Properties of the Delafossite $LaCuO_2$. *Journal of Physics and Chemistry of Solids*, **70**, 1132-1136. https://doi.org/10.1016/j.jpcs.2009.06.011